

Doppler Signature Analysis of Over-The-Horizon Radar Signals with Target Altitude Perturbation

Ammar Ahmed and Yimin D. Zhang
Department of Electrical and Computer Engineering
Temple University
Philadelphia, PA 19122, USA

Braham Himed
Distributed RF Sensing Branch
Air Force Research Laboratory
WPAFB, OH 45433, USA

Abstract—In this paper, we examine the Doppler signatures of local-multipath signals in over-the-horizon radar for a target that moves with a constant horizontal velocity but experiences altitude perturbation. In practice, the target altitude may deviate from its scheduled altitude due to, e.g., flight dynamics. After describing the Doppler signatures for a target that maintains a constant altitude without perturbation, we develop the mathematical framework for target Doppler signature analysis that includes target altitude perturbations. It is observed that altitude variations result in spreading of Doppler frequencies, and the bias is associated with the average target altitude. It is observed that, for mild target altitude perturbations, existing analysis methods remain effective for local-multipath Doppler frequency estimation. The Doppler frequency estimation capability and performance are verified using simulation results.

Keywords: Doppler parameter estimation, fractional Fourier transform, over-the-horizon radar, target perturbation.

I. INTRODUCTION

Sky-wave over-the-horizon radar (OTHR) systems provide early warning capability by enabling long-range surveillance of targets that are far beyond the limit of the earth horizon [1–5]. These systems monitor non-line-of-sight targets by exploiting the ionospheric reflections of narrowband signals whose bandwidth is determined based on the ionospheric conditions. This fact makes accurate target geo-location, particularly the estimation of target altitude, very challenging.

Considerable efforts have been invested to estimate the target parameters in OTHR [6–8]. An important parameter for target recognition and classification is target altitude, and significant attention has been dedicated to achieve this goal [9–13]. In this context, altitude estimation using a matched-field approach was presented in [9] by exploiting multiple OTHR dwells and the altitude-dependent structure of the micro-multipath rays resulting from reflections local to the target. This approach was further extended in [10] to estimate the altitude rate of the target by investigating the effects of constant altitude rate on the micro-multipath Doppler frequencies. A state-space model-based generalized altitude estimation was presented in [11] where the effect of random ionospheric and target motion, which degrades the dwell-to-dwell predictability of target returns, was also considered. A study related to the experimental validation of target altitude estimation by exploiting multipath propagation model was reported in [12].

Contrary to the aforementioned approaches, instantaneous target altitude estimation by employing non-stationary signal analysis of the time-varying multipath Doppler signature was considered in [13], where the initial state of target parameters was obtained using the maximum a-posteriori criterion. It was observed that the Doppler difference of the received multipath signals can be exploited to estimate target altitude. However, due to the proximity of the Doppler components in the spectral domain, achieving improved Doppler frequency resolution remained a challenging problem in order to achieve effective target altitude estimation [14–18]. Doppler analysis was recently considered for enhanced altitude estimation in the presence of ionospheric layer motion when target maintains a constant altitude [19]. In addition, the existence of both ordinary and extraordinary modes of ionospheric propagation leads to an increased number of Doppler frequency components to be resolved [20, 21].

In practice, air targets experience altitude perturbations due to flight dynamics and the external atmospheric environment [22, 23]. As a result, multipath Doppler signatures of a target deviate from the signal model originally developed for targets without such altitude perturbation. In this paper, we investigate the effect of such target altitude perturbation on the resulting Doppler signatures. We provide mathematical formulations which quantify the Doppler frequency estimation error due to target perturbations. It is observed that the target altitude perturbation results in Doppler signature spreading but does not affect the average Doppler component and has a limited impact on the difference Doppler component. Further it is seen that, for a scenario with mild target altitude perturbations, existing methods remain effective for local-multipath Doppler frequency estimation. The Doppler frequency estimation capability and performance of the proposed methods are verified using simulation results.

II. SIGNAL MODEL

A. Multipath Propagation Geometry

Consider a target that flies with a constant horizontal velocity either towards or away from an OTHR system operating in a pseudo-monostatic mode. The propagation paths in a simplified flat-earth setting are shown in Fig. 1, where the targets and propagation paths below the ionosphere layer are physically present, whereas those above the ionosphere layer are their images due to ionosphere and ground reflections and are included for convenience of slant-range computations. In Fig. 1, H is the height of the ionosphere layer which is assumed constant and its coarse estimate is available from ionosonde monitoring. In addition, the time-varying aspect

The work of A. Ahmed and Y. D. Zhang is supported in part by a contract with Matrix Research, Inc. for research sponsored by the Air Force Research Laboratory under Contract FA8650-14-D-1722. The work of Y. D. Zhang is also supported in part by a contract with Altamira Technologies Corp. for research sponsored by the Air Force Research Laboratory under Contract FA8650-18-C-1055.

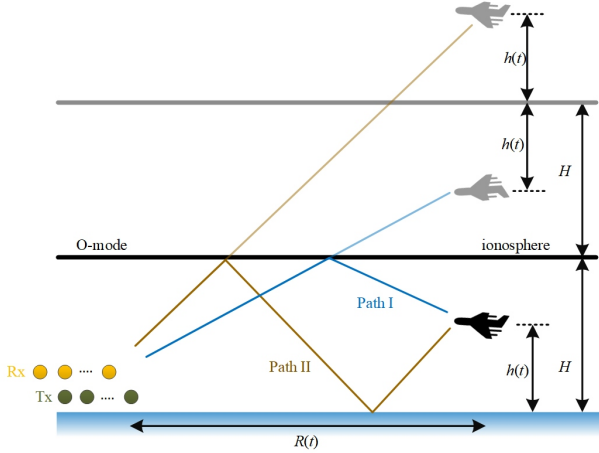


Fig. 1: Flat-earth local-multipath propagation model of OTHR.

of target ground range with respect to the radar antennas is denoted by $R(t)$, and $h(t)$ denotes the target altitude. For notational convenience, the explicit notation (t) is omitted when describing time-varying target ground range and altitude, as well as the associated Doppler frequencies.

The OTHR signals reflected by the target and received at the OTHR radar receivers follow multiple round-trip paths due to their reflections from the ionosphere and the earth surface. As illustrated in Fig. 1, the specular earth and ionosphere reflections result in two different propagation paths for each of the transmit and receive OTHR signals, yielding three distinct round-trip paths. For the first round-trip path, both transmit and receive OTHR signals propagate along Path I, denoted as $[l_1, l_1]$. Similarly, for the second round-trip path $[l_2, l_2]$ follows Path II for both ways. The third round-trip path uses different forward and return paths, i.e., $[l_1, l_2]$ and $[l_2, l_1]$.

From Fig. 1, we can calculate the one-way slant ranges l_1 and l_2 of Path I and Path II in terms of the ionosphere height H , target ground range R , and target altitude h , as [8]:

$$l_1 = (R^2 + (2H - h)^2)^{\frac{1}{2}} = R \left(1 + \frac{4H^2 + h^2 - 4Hh}{R^2} \right)^{\frac{1}{2}}, \quad (1a)$$

$$l_2 = (R^2 + (2H + h)^2)^{\frac{1}{2}} = R \left(1 + \frac{4H^2 + h^2 + 4Hh}{R^2} \right)^{\frac{1}{2}}. \quad (1b)$$

In order to gain insightful observations of the relationship between the Doppler frequencies and the target motion, we exploit the first-order Taylor series expansion on Eq. (1). Under the commonly satisfied assumption $R \gg H \gg h$, we obtain the following simplified expressions of one-way slant ranges:

$$l_1 \approx R + \frac{2H^2 - 2Hh}{R}, \quad l_2 \approx R + \frac{2H^2 + 2Hh}{R}. \quad (2)$$

B. Multipath Doppler Signatures

The slant ranges of the three round-trip paths (path I: $[l_1, l_1]$, path II: $[l_2, l_2]$, and path III: $[l_1, l_2]$ or $[l_2, l_1]$) can be respectively represented as:

$$L_1 = 2l_1, \quad L_2 = 2l_2, \quad L_3 = l_1 + l_2. \quad (3)$$

The Doppler signatures corresponding to the three round-trip paths can be expressed as:

$$f_{D,i} = -\frac{f_c}{c} \frac{dL_i}{dt}, \quad i = 1, 2, 3, \quad (4)$$

where f_c denotes the carrier frequency of the OTHR signal and c is the velocity of the electromagnetic wave.

III. TARGET DOPPLER CHARACTERISTICS

In this section, we investigate the local-multipath Doppler frequencies of a target and the effect of target altitude perturbation. For this purpose, we first consider that the target is moving at a constant altitude h , and the effect of target altitude perturbation on the resulting Doppler signatures is then examined.

A. Target with a Constant Altitude

A target with a constant altitude is characterized by $\dot{h} = dh/dt = 0$. In this case, using the approximations in Eq. (2), the derivatives of one-way slant ranges are expressed as:

$$\frac{dl_1}{dt} \approx \dot{R} - \frac{2H\dot{R}}{R^2} (H - h), \quad \frac{dl_2}{dt} \approx \dot{R} - \frac{2H\dot{R}}{R^2} (H + h). \quad (5)$$

Note that the target velocity \dot{R} takes a positive value when the target ground range increases with time.

Using Eq. (4), we can find the Doppler frequencies due to the three round-trip paths as follows:

$$f_{D,1} = \bar{f}_D + \Delta f_D, \quad f_{D,2} = \bar{f}_D - \Delta f_D, \quad f_{D,3} = \bar{f}_D, \quad (6)$$

where

$$\bar{f}_D = -\frac{f_c}{c} \frac{d(l_1 + l_2)}{dt} \approx -\frac{2f_c}{c} \dot{R} + \frac{4f_c H^2}{cR^2} \dot{R}, \quad (7a)$$

$$\Delta f_D = -\frac{f_c}{c} \frac{d(l_1 - l_2)}{dt} \approx \frac{4f_c h}{cR^2} H \dot{R}. \quad (7b)$$

From the above equation, it is clear that the Doppler signatures for round-trip paths I and II are symmetric and wrap around the Doppler signature of round-trip path III. The average Doppler component, \bar{f}_D , is shared by all three round-trip paths, whereas the small frequency difference between the Doppler signatures corresponding to different paths is characterized by Δf_D .

B. Target with Altitude Perturbations

When a target, which maintains constant altitude during the flight experiences altitude perturbations, the derivative of the target altitude \dot{h} deviates from zero. In this case, the derivatives of one-way slant ranges become:

$$\frac{dl_1}{dt} \approx \dot{R} - \frac{2H^2}{R^2} \dot{R} - \frac{2H}{R^2} (R\dot{h} - \dot{R}h), \quad (8a)$$

$$\frac{dl_2}{dt} \approx \dot{R} - \frac{2H^2}{R^2} \dot{R} + \frac{2H}{R^2} (R\dot{h} - \dot{R}h). \quad (8b)$$

The corresponding instantaneous Doppler frequencies corresponding to the three round-trip paths are expressed in Eq. (6) with \bar{f}_D and Δf_D are now given as:

$$\bar{f}_D = -\frac{f_c}{c} \frac{d(l_1 + l_2)}{dt} \approx -\frac{2f_c}{c} \dot{R} + \frac{4f_c H^2}{cR^2} \dot{R}, \quad (9a)$$

$$\Delta f_D = -\frac{f_c}{c} \frac{d(l_1 - l_2)}{dt} \approx \frac{4f_c H}{cR^2} (\dot{R}h - R\dot{h}). \quad (9b)$$

TABLE I: Key Parameters (unless otherwise specified)

Parameter	Notation	Value
Initial range	R	2,500 km
Ionosphere height	H	350 km
Target altitude	h	20 km
Target velocity (horizontal)	\dot{R}	-500 m/sec
Carrier frequency	f_c	16 MHz
Pulse repetition frequency	f_s	140 Hz
Signal-to-noise ratio	SNR	-15 dB
Coherent processing interval	T	80 s

By comparing Eqs. (7) and (9), we see that the perturbation in the target altitude only changes the difference Doppler component Δf_D . If the target altitude perturbation is relatively small, the instantaneous vertical velocity of the target will introduce a bias in the difference Doppler component given by Eqs. (7b) and (9b) as:

$$e(\Delta f_D) \approx \frac{4f_c H}{cR} \dot{h}. \quad (10)$$

Fig. 2 illustrates the variation in Δf_D with respect to the perturbation in target altitude h for the parameters listed in Table I. It is observed that, for a small variation in the target altitude, the corresponding Doppler frequencies do not change drastically. For an altitude variation of 0.5 m/sec, the bias in the resulting difference Doppler components, assuming constant altitude, is approximately 0.0045 Hz, which is about 3.8% of the actual value of Δf_D .

Note that the perturbation \dot{h} varies with time and, therefore, the corresponding perturbation in Δf_D will also vary with time, resulting in the spreading of Doppler frequencies in the spectral domain. Fractional Fourier transform (FrFT)-based methods, described in Section IV, can be used to estimate the Doppler signatures if \dot{h} is small such that it does not result in substantial Doppler spreading. Moreover, if $\mathbb{E}[\dot{h}] = 0$ during the coherent processing interval, where $\mathbb{E}[\cdot]$ denotes the expectation operator, $\mathbb{E}[e(\Delta f_D)]$ is unbiased.

IV. DOPPLER SIGNATURE ANALYSIS

Assuming a constant ionosphere altitude H and utilizing the fact that $\dot{h} \ll \dot{R}$, we can deduce from Eq. (7) that \dot{f}_D and $\Delta \dot{f}_D$ are constant with respect to time, given by

$$\dot{f}_D \approx -\frac{8f_c}{c} \frac{H^2}{R^3} \dot{R}^2, \quad \Delta \dot{f}_D \approx -\frac{8f_c}{c} \frac{Hh}{R^3} \dot{R}^2. \quad (11)$$

Since $h \ll H \ll R$, $\Delta \dot{f}_D$ can be approximated as 0. Moreover, \dot{f}_D is a constant. Therefore, the three Doppler signatures can be well characterized as three parallel chirps (also known as linear frequency modulated signals) with a small chirp rate \dot{f}_D .

The received signal at the OTHR is expressed as:

$$x(t) = A_1 e^{j(2\pi \int_0^T (\bar{f}_D + \Delta f_D) dt + \phi_1)} + A_2 e^{j(2\pi \int_0^T (\bar{f}_D - \Delta f_D) dt + \phi_2)} + A_3 e^{j(2\pi \int_0^T \bar{f}_D dt + \phi_3)} + n(t), \quad (12)$$

where A_i denotes the respective signal amplitudes for the i th chirp signal for $i = 1, 2, 3$, ϕ_i is the corresponding initial

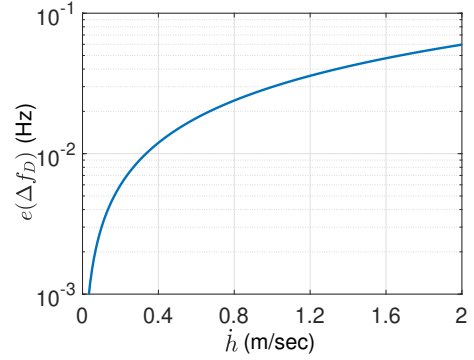


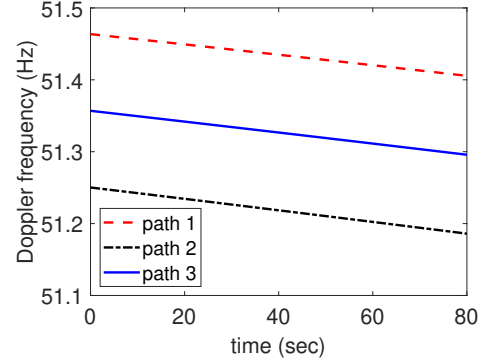
Fig. 2: Instantaneous variation in Δf_D with respect to perturbation in target altitude.

phase, and $n(t)$ is the additive white Gaussian noise, assumed to be circularly complex independent with zero-mean.

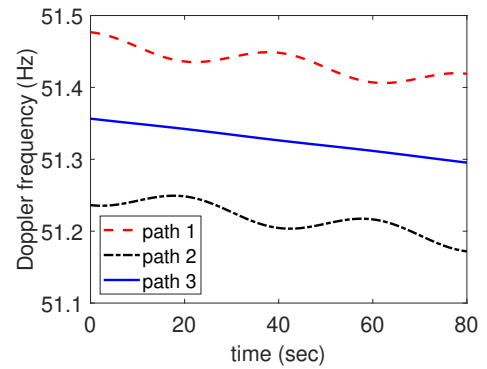
The spectrogram of the received signal $x(t)$, which is defined as the magnitude square of the short-time Fourier transform, is expressed as

$$S(t, f) = \left| \int_{-\infty}^{\infty} |x(u)|^2 g(t-u) \exp(-j2\pi fu) du \right|^2, \quad (13)$$

where $g(t)$ is a window function.

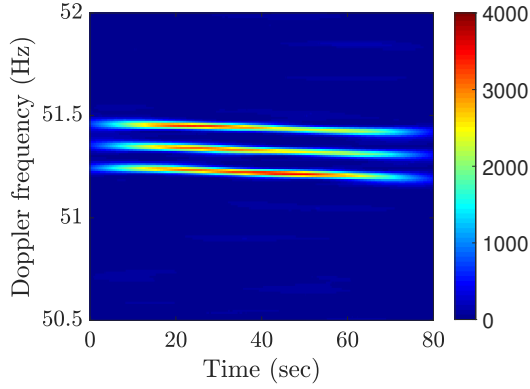


(a) Stable target altitude

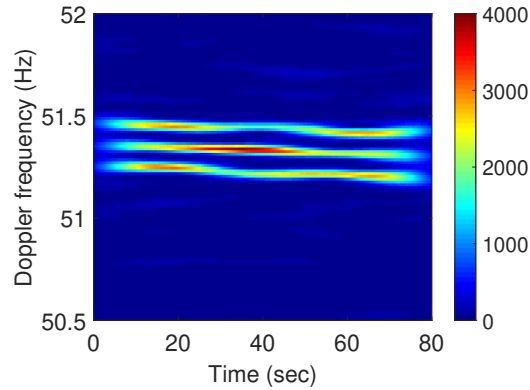


(b) Perturbed target altitude, $h = 20 \times 10^3 + 3 \sin(0.05\pi t)$ m

Fig. 3: Comparison of Doppler signatures for stable and perturbed target altitude.



(a) Stable target altitude



(b) Perturbed target altitude, $h = 20 \times 10^3 + 3 \sin(0.05\pi t)$ m

Fig. 4: Spectrograms of Doppler signatures for stable and perturbed target altitude.

Since the received signals are regarded as three parallel chirps, several strategies developed for chirp parameter estimation can be exploited to determine the chirp parameters. For instance, we can use FrFT to estimate the chirp rate and frequency separation of the Doppler components. The α -angle FrFT of the signal $x(t)$, denoted by $\mathcal{X}_\alpha(u)$, is expressed as [24]:

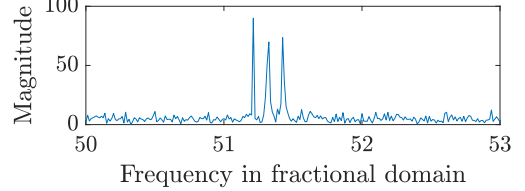
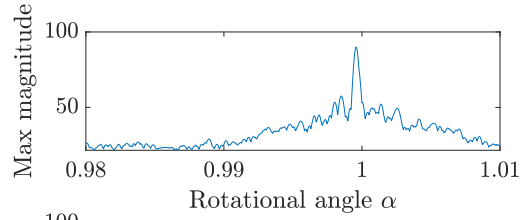
$$\mathcal{X}_\alpha(u) = \int_{-\infty}^{\infty} x(t) \mathcal{K}_\alpha(t, u) dt, \quad (14)$$

where

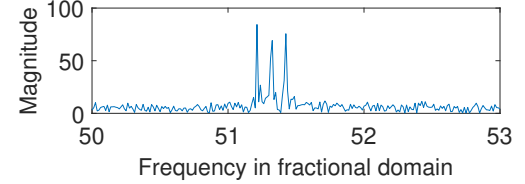
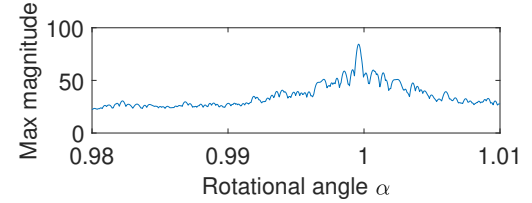
$$\mathcal{K}_\alpha(t, u) = \begin{cases} \sqrt{\frac{1 - j \cot(\phi)}{2\pi}} e^{j \frac{u^2}{2} \cot(\phi)} \\ \quad \times e^{j \frac{t^2}{2} \cot(\phi)} e^{-j u \csc(\phi)}, & \phi \neq k\pi, \\ \delta(t - u), & \phi = 2k\pi, \\ \delta(t + u), & \phi + \pi = 2k\pi, \end{cases}$$

k is a non-negative integer, u is the angular fractional frequency, and $\phi = \alpha\pi/2$. Once an optimal rotation angle α_{opt} , which aligns the three chirps in the fractional Fourier domain, is estimated, we can determine the chirp rate using the following equation [24]:

$$\hat{\mu} = -\cot\left(\alpha_{\text{opt}} \frac{\pi}{2}\right) \frac{f_s^2}{N}, \quad (15)$$



(a) Stable target altitude



(b) Perturbed target altitude, $h = 20 \times 10^3 + 3 \sin(0.05\pi t)$ m

Fig. 5: FrFT of Doppler signatures for stable and perturbed target altitude.

where $\hat{\mu}$ is the estimated chirp rate of the three Doppler components, f_s is the pulse repetition frequency of OTHR, $N = f_s T$ is the number of time samples used for calculating the FrFT, and T is the coherent processing interval.

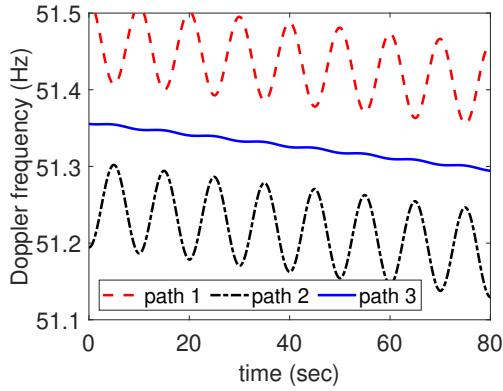
The actual centroid frequency f_{center} of the chirp signal corresponding to its peak fractional domain frequency f_{frft} can be found as [24]:

$$f_{\text{center}} = \frac{f_{\text{frft}}}{\sin(\alpha_{\text{opt}} \pi / 2)}, \quad (16)$$

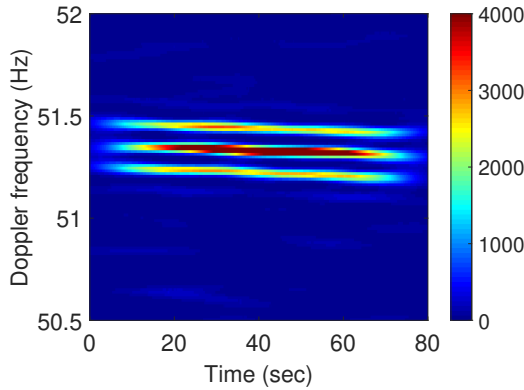
where $f_{\text{frft}} = u_{\text{peak}} f_s / \pi$ and u_{peak} is the estimated peak angular frequency of the individual chirp in the fractional domain.

V. SIMULATION RESULTS

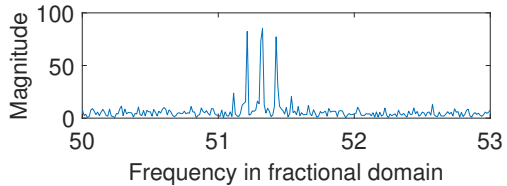
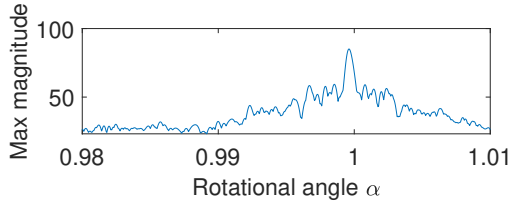
In the simulations, we compare the Doppler frequencies of the received OTHR signals for constant target altitude with those in the presence of target altitude perturbation. For this purpose, the effect of both the maximum target altitude perturbation as well as the perturbation rate on the resulting Doppler signatures is investigated. We consider a target travelling at an altitude of 20 km at the initial range of 2,500 km. The ionosphere height is assumed to be 350 km. The OTHR is operating at a carrier frequency of 16 MHz with



(a) Actual Doppler signatures



(b) Spectrogram

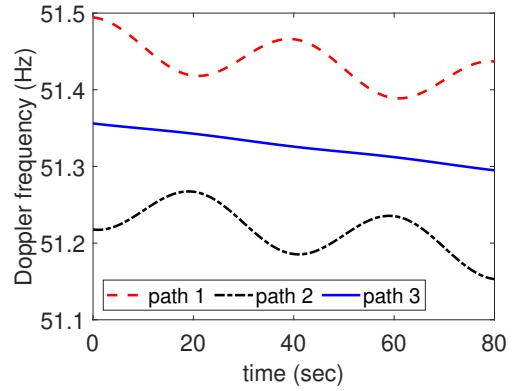


(c) FrFT

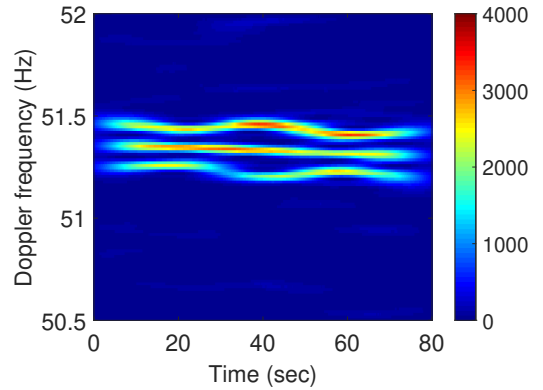
Fig. 6: Doppler signature analysis of multipath signals for high target altitude perturbation ($h = 20 \times 10^3 + 3 \sin(0.2\pi t)$ m).

a pulse repetition frequency of 140 Hz. The input signal-to-noise ratio (SNR) for each Doppler component is assumed to be the same and equal to -15 dB. The complete set of parameters is illustrated in Table I unless otherwise specified.

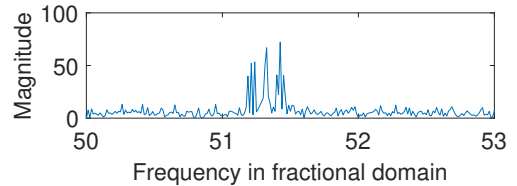
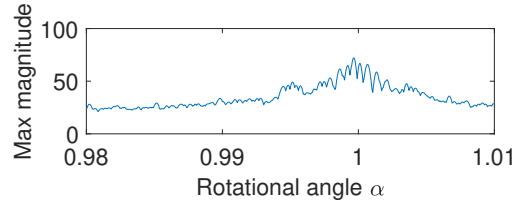
As a baseline for comparison, Fig. 3(a) shows the target Doppler signatures without altitude perturbation. Now, we assume an altitude perturbation model of $h = 20 \times 10^3 + 3 \sin(0.05\pi t)$ m which accounts for a maximum change of 6 m in target altitude throughout the radar coherent processing interval. The corresponding Doppler signatures are depicted



(a) Actual Doppler signatures



(b) Spectrogram



(c) FrFT

Fig. 7: Doppler signature analysis of multipath signals for high target altitude perturbation ($h = 20 \times 10^3 + 7 \sin(0.05\pi t)$ m).

in Fig. 3(b). Note that the target elevation velocity \dot{h} and the Doppler perturbation are functions of both the maximum altitude perturbation and the perturbation rate. The corresponding spectrograms for both cases of stable and perturbed target altitudes are shown in Fig. 4. We observe that a benign change of ± 3 m in the target altitude does not significantly deviate the Doppler frequency signature of the three multipath components from chirp structures, but the amplitudes of the $f_{D,1}$ and $f_{D,2}$ components are slightly reduced due to the frequency spreading in those Doppler components. The FrFT results for

both cases of stable and perturbed target altitudes are shown in Fig. 5. We observe that the estimation of α_{opt} is comparatively challenging for the case of altitude perturbation as the ratio between the mainlobe peak of α to its sidelobe amplitude becomes smaller for this case compared to the stable altitude case. On the other hand, Doppler frequency estimation has no significant effect.

Next, we increase the frequency of target altitude perturbation and investigate its impact on the resulting Doppler signatures. Fig. 6 shows the results for high-frequency target altitude perturbation of $h = 20 \times 10^3 + 3 \sin(0.2\pi t)$ m, i.e., the perturbation radian frequency is increased from 0.05π to 0.2π , whereas the range of amplitude perturbation is kept unchanged at ± 3 m. It is observed that the frequency of perturbation does not have a significant effect on the Doppler frequency estimation for mild altitude perturbation.

In the last simulation, we investigate the effect of high-amplitude altitude perturbation on the three Doppler signatures. For this purpose, we increase the altitude perturbation range from ± 3 m to ± 7 m such that $h = 20 \times 10^3 + 7 \sin(0.05\pi t)$ m. In this case, Fig. 7(a) shows the actual Doppler signatures of the three multipath components and Fig. 7(b) shows the corresponding spectrogram of the received signal. It is observed that the spectrogram of the three Doppler signatures significantly deviates from the spectrogram of the three parallel chirps. Fig. 7(c) shows the FrFT of the corresponding Doppler signatures. It is observed that, due to the large altitude perturbation, it becomes difficult to confidently estimate the chirp rate and the Doppler signatures corresponding to the three multipath signals.

VI. CONCLUSION

In this paper, we have analyzed the Doppler frequencies of target signals in OTHR when the target experiences altitude perturbations. It is observed that the altitude variation spreads the Doppler signatures in the spectral domain. This potentially leads to difficulty in frequency or chirp rate estimation due to basis mismatch. However, for small target altitude perturbations, this mismatch remains insignificant and Doppler frequency estimation is still possible without a significant error.

VII. REFERENCES

- [1] M. Headrick and M. I. Skolnik, "Over-the-horizon radar in the HF band," *Proc. IEEE*, vol. 62, no. 6, pp. 664–673, June 1974.
- [2] L. F. McNamara, *The Ionosphere: Communications, Surveillance, and Direction Finding*, Krieger Publishing Company, 1999.
- [3] G. J. Frazer, Y. Abramovich, B. A. Johnson, "Use of adaptive non-causal transmit beamforming in OTHR: Experimental results," in *Proc. Int. Conf. Radar*, Adelaide, Australia, Sept. 2008, pp. 311–316.
- [4] J. M. Headrick and S. J. Anderson, "HF over-the-horizon radar," Chapter 20 in M. Skolnik (ed.), *Radar Handbook, 3rd Ed.* McGraw-Hill, 2008.
- [5] G. A. Fabrizio, *High Frequency Over-the-Horizon Radar: Fundamental Principles, Signal Processing, and Practical Applications*. McGraw-Hill, 2013.
- [6] K. Bell, "MAP-PF multi-mode tracking for over-the-horizon radar," in *Proc. IEEE Radar Conf.*, Atlanta, GA, May 2012, pp. 326–331.
- [7] K. Lu, and X. Liu, "Enhanced visibility of maneuvering targets for high-frequency over-the-horizon radar," *IEEE Trans. Antennas Propag.*, vol. 53, no. 1, pp. 404–411, Jan. 2005.
- [8] Y. D. Zhang, M. G. Amin, and G. J. Frazer, "High-resolution time-frequency distributions for manoeuvring target detection in over-the-horizon radars," *IEE Proc.-Radar Sonar Navig.*, vol. 150, no. 4, pp. 299–304, Aug. 2003.
- [9] M. Papazoglou and J. L. Krolik, "Matched-field estimation of aircraft altitude from multiple over-the-horizon radar revisits," *IEEE Trans. Signal Process.*, vol. 47, no. 4, pp. 966–976, April 1999.
- [10] M. Papazoglou and J. L. Krolik, "Estimation of aircraft altitude and altitude rate with over-the-horizon radar," in *Proc. IEEE Int. Conf. Acoust. Speech Signal Process.*, Phoenix, AZ, March 1999, pp. 2103–2106.
- [11] R. H. Anderson, S. Kraut, and J. L. Krolik, "Robust altitude estimation for over-the-horizon radar using a state-space multipath fading model," *IEEE Trans. Aerospace Electron. Syst.*, vol. 39, no. 1, pp. 192–201, Mar. 2003.
- [12] J. Prashifka, L. J. Durbridge and J. Lane, "Investigation of target altitude estimation in skywave OTH radar using a high-resolution ionospheric sounder," in *Proc. Intl. Radar Conf.*, Bordeaux, France, Oct. 2009, pp. 1–6.
- [13] Y. D. Zhang, J. J. Zhang, M. G. Amin, and B. Himed, "Instantaneous altitude estimation of maneuvering targets in over-the-horizon radar exploiting multipath Doppler signatures," *EURASIP J. Adv. Signal Process.*, vol. 2013, no. 2013:100, pp. 1–13, May 2013.
- [14] C. Ioana, M. G. Amin, Y. D. Zhang, and F. Ahmad, "Characterization of Doppler effects in the context of over-the-horizon radar," in *Proc. IEEE Radar Conf.*, Washington, D.C., May 2010, pp. 506–510.
- [15] C. Ioana, Y. D. Zhang, M. G. Amin, F. Ahmad, G. Frazer, and B. Himed, "Time-frequency characterization of micro-multipath signals in over-the-horizon radar," in *Proc. IEEE Radar Conf.*, Atlanta, GA, May 2012, pp. 671–675.
- [16] I. Djurovic and Y. D. Zhang, "Accurate parameter estimation of over-the-horizon radar signals using RANSAC and MUSIC algorithms," *Prog. Electromagn. Res. M*, vol. 67, pp. 85–92, April 2018.
- [17] Y. D. Zhang and B. Himed, "Multipath Doppler difference estimation in over-the-horizon radar," in *Proc. IEEE Radar Conf.*, Oklahoma City, OK, April 2018.
- [18] V. S. Amin, Y. D. Zhang, and B. Himed, "Modified Viterbi-based local-multipath Doppler difference estimation in over-the-horizon radar," in *Proc. Asilomar Conf. Signals, Systems, Computers*, Pacific Grove, CA, Oct. 2021.
- [19] Y. D. Zhang, A. Ahmed, and B. Himed, "Target altitude estimation in over-the-horizon radar," *IEEE Access*, in press.
- [20] A. Ahmed, Y. D. Zhang, and B. Himed, "Doppler signature analysis of mixed O/X-mode signals in over-the-horizon radar," in *Proc. IEEE Int. Radar Conf.*, Rockville, MD, April 2020.
- [21] A. Ahmed, Y. D. Zhang, and B. Himed, "Doppler signature separation of mixed O/X-mode over-the-horizon radar signals," in *Proc. IEEE Radar Conf.*, Florence, Italy, Sep. 2020.
- [22] B. E. Vivaldi, "The effect of crosswind and turbulence in mental workload and pilot tracking performance," MS Thesis, Department of Human Factors & Systems, Embry-Riddle Aeronautical University, Daytona Beach, FL, 2004.
- [23] Y. Wang and B. Geerts, "Estimating the evaporative cooling bias of an airborne reverse flow thermometer," *J. Atmos. Oceanic Technol.*, vol. 26, no. 1, pp. 3–21, Jan. 2009.
- [24] H. M. Ozaktas, M. A. Kutay, and Z. Zalevsky, *The Fractional Fourier Transform: With Applications in Optics and Signal Processing*. Wiley, 2001.